Chapter 10

Luminescence from TiO_2 Nanotubes and Related Nanostructures Investigated Using Synchrotron X-Ray Absorption Near-Edge Structure and X-Ray Excited Optical Luminescence

Lijia Liu and Tsun-Kong Sham

Additional information is available at the end of the chapter

http://dx.doi.org/10.5772/intechopen.72856

Abstract

Understanding the optical property of nanostructured TiO_2 is crucial for their use in a variety of applications such as solar cells, photocatalysis, and light emitting devices. Herein, we introduce the use of synchrotron radiation-based spectroscopic techniques: X-ray absorption near-edge structure (XANES) and X-ray excited optical luminescence (XEOL) in analyzing the luminescence properties of anodized TiO_2 nanotubes (TiO_2 NT) and related materials. A description on the spectroscopic technique is first given, including conventional XANES-XEOL combined analysis and a more recently developed 2D XANES-XEOL probing technique. We then discuss several examples of analyzing the luminescence mechanism of TiO_2 NT using XANES and XEOL technique, which are the phase transformation accompanied luminescence, luminescence from TiO_2 NT hierarchical structure, and metal particle–coated TiO_2 NT.

Keywords: TiO_2 nanotubes, luminescence, X-ray absorption near-edge structure, X-ray excited optical luminescence, Ti L-edge, phase transformation, hierarchical structure, metal nanoparticles

1. Introduction

The properties and potential applications of TiO_2 nanotubes (TiO_2NT) have been actively researched. Because of their 1D tubular structure, they provide an ideal media for highly directional charge transport, and are explored in many photoelectrochemical applications such as solar cells [1], photocatalysis [2], sensors [3], and battery electrodes [4]. Besides, the high biocompatibility of TiO_2 also makes it an excellent coating for substrate for depositing bioactive species [5].

In TiO_2, Ti and O form distorted octahedra, and the different octahedra packing leads to various crystal phases, such as anatase, rutile, brookite, and B-phase. Anatase is a low-density metastable phase, and contains catalytically active crystal facets, and a relatively loose structure. Rutile is the most thermodynamically stable phase with the highest density. Brookite is less common, although it has been reported that it is an intermediate phase during phase transformation [6]. B-phase has a highly distorted structure, which commonly occurs during hydrothermal synthesis, and is a good candidate as ion battery electrode [7, 8]. The crystal phases are highly sensitive to temperature, and with increasing temperature, phase transformation occurs. Under mild calcination temperature (200–600°C), TiO_2 NT forms an anatase phase, while higher calcination temperature induces an irreversible phase transformation to rutile [9, 10]. Studies on various TiO_2 nanostructures, such as nanoparticles, nanowires, thin films, suggest that the phase transformation temperature highly depends on the morphology and composition of materials [11–13]. In fact, with well-controlled synthesis, an anatase-rutile composite can provide better catalytic performance than single-phase TiO_2 [14, 15]. TiO_2 nanotubes produced electrochemically from a Ti foil are usually in an amorphous form and transform to anatase phase with calcination temperature below 600°C. Although the exact transformation temperature can be adjusted by nanotube size or introducing dopant, at higher temperature, all anatase TiO_2 eventually transforms to the thermodynamically stable rutile phase.

Synthesis strategies of TiO_2 nanotubes have been developed for more than a decade, and they can now be synthesized with well-controlled diameters, lengths, wall thicknesses, and surface roughness [16, 17]. Hydrothermal, anodization, and template-assisted methods are successful in producing TiO_2 NT. Besides, some complex structures such as tube-in-tube [18], particle-decorated [19], and hierarchical structures [20] have also been reported. Such structures exhibit unusual electronic and optical properties and their potential applications in various fields are still actively explored.

The luminescence properties of TiO_2 are strongly dependent on crystal phases and the quality of the crystallinity. For example, upon X-ray excitation, anatase usually exhibits a visible green emission at around 550 nm, while rutile shows an intense near-IR emission at around 800 nm. Both emissions have energies lower than the bandgap, so they both are of a defect origin. The visible green emission is highly sensitive to surface structure and the presence of impurities, and is affected by modifying the surface condition of TiO_2 [21, 22], while the near IR emission is relatively stable. In addition, a recent work reports that weak bandgap emission has been observed from ultra-small amorphous TiO_2 nanograss structures (unzipped TiO_2 NT) [20]. It is thus crucial to establish a connection between the observed luminescence and the structure of the materials.

The conventional way of detecting luminescence is photoluminescence, PL (often called fluorescence), which uses visible or UV light as an excitation source. In wide bandgap semiconductors such as TiO_2, valence electrons are excited to the conduction band, and radiative recombination is recorded with a spectrometer. The experiment setup is readily available, and it is a direct probe of the emission from a sample. However, since the electrons are from the entire valence band, it lacks element specificity. In other words, we know at what wavelength the sample is emitting light, but we do not know what is responsible for it. In this chapter, we

highlight a characterization technique that probes luminescence of materials with element and site specificity: X-ray absorption near-edge structure (XANES) in combination with X-ray excited optical luminescence (XEOL). It is conducted at synchrotron radiation facility, and utilizes a tunable X-ray to monitor the luminescence from material upon core electron excitation. XANES-XEOL analysis, especially in the soft X-ray range, has proven an effective technique in studying the luminescence mechanism of various light-emitting materials, such as ZnO nanowires [23], and GaN-ZnO solid solution [24].

The content of the chapter is organized as follows: we first give an overview of the methods for producing highly oriented nanotubes by anodization, followed by an introduction of the XANES and XEOL techniques. Then, we use two sets of examples to demonstrate how XANES-XEOL method is applied in analyzing the luminescence mechanism of TiO_2 NT: first is the phase transformation associated luminescence and second is the TiO_2 hierarchical structures and doped structures. Finally, an outlook of this material and the use of synchrotron X-ray spectroscopy are given.

2. Material synthesis and characterization techniques

2.1. Electrochemical anodization

TiO_2 NT discussed in this chapter is synthesized using electrochemical anodization, which is a well-developed synthetic strategy for producing highly oriented TiO_2 nanotube arrays grown on Ti foils. **Figure 1a** shows a schematic layout of the anodization setup. A piece of Ti foil is used as the anode, and a piece of Pt foil is used as the cathode. The two electrodes are immersed in an ethylene glycol-based electrolyte which contains F^- (from either HF or NH_4F), and a voltage of several tens of volts is applied [17]. After certain duration, TiO_2 NT will form on the Ti foil, with a typical morphology, shown in **Figure 1b**. By controlling the electrolyte composition, voltage, and the duration of the anodization, TiO_2 NT can be produced with controlled diameter, length, and wall thickness. The as-formed TiO_2 NT has an amorphous structure, so post-annealing is often required to produce TiO_2 NT of desired crystal phases.

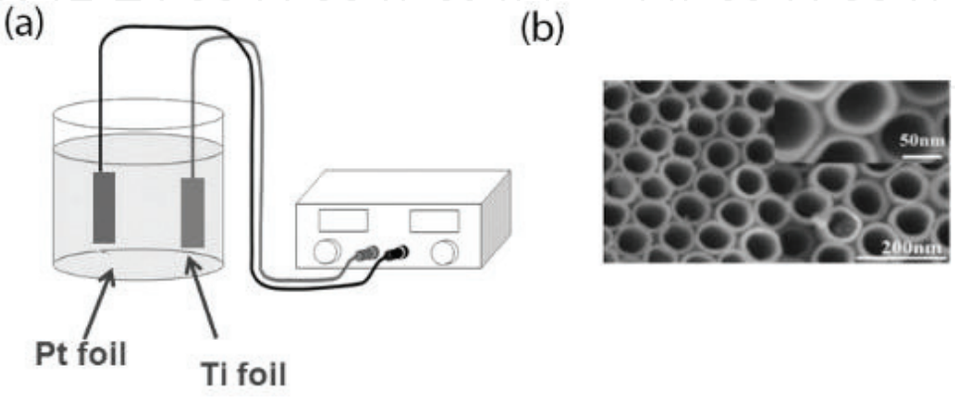

Figure 1. (a) Experimental setup of anodization and (b) a typical top-view SEM image of as-prepared TiO_2NT.

2.2. X-ray absorption near-edge structure

X-ray absorption near-edge structure (XANES) is a technique that probes the local chemical environment of an element in a compound. It utilizes a tunable X-ray source from synchrotron to excite a core electron of the element of interest and monitor the modulation of the absorption coefficient at the absorption edge. Once the energy of the incoming X-ray is sufficient to induce a core electron transition, there is a sharp increase in the absorption coefficient, which is called an "edge" in the corresponding absorption spectrum. The energy position of the "edge" marks the onset energy where electronic transition occurs. Above the edge, spectrum usually exhibits rich features, which are due to multiple scattering between the outgoing electron and the electrons from surrounding atoms. These features are regarded as the "fingerprint" of the material, since they are highly sensitive to the local geometry and the species of neighboring atoms. In short, the photoelectron propagates away from the absorbing atom, samples the neighboring atoms via backscattering, brings the information back to the absorbing atom, the information appears as spectral features in the XANES. In recent years, XANES has been recognized as a valuable technique and has been used to analyze various novel nanomaterials used in catalysis [25], solar cells [26], batteries [27], and so on. It can provide element specific chemical structure with both surface and bulk sensitivity by selecting different detection modes (i.e. total electron yield (TEY) for measuring a few angstroms to nanometers on the surface, and fluorescence yield (FY) for measuring several hundreds of nanometers (as for TiO_2)) with soft X-rays and a few micrometers under the surface. This advantage makes XANES an ideal non-destructive probe for analyzing layered, core-shell, or heterostructures. In addition, it can be combined with in situ facility to study the involvement of chemical species during chemical reaction in catalysis [28] or electrochemical cycling [29]. When using a micro- or nanosized probing beam, XANES can also be conducted with site sensitivity, to achieve chemical structure mapping of soil [30], biofilms [31], or nanocomposite [32].

The rich information in XANES is obtained by excitation of core electrons in the element of interest and at appropriate energy levels. As for TiO_2, XANES collected at three edges are of particular interest. The Ti $L_{3,2}$-edge is the excitation of Ti 2p electrons ($2p_{3/2}$ for L_3, and $2p_{1/2}$ for L_2) to the previously unoccupied electronic states with d and s characters. The Ti K-edge, which is the excitation of Ti 1s electron, and the O K-edge, which excites the O 1s electron into previously unoccupied p states. Since the conduction band of TiO_2 is mainly composed of hybridized Ti 3d and O 2p states, which makes the Ti $L_{3,2}$- and the O K-edges ideal for the investigate the structure and bonding, hence chemical reactivity of TiO_2. The Ti K-edge, on the other hand, is also used in identifying Ti-based species, but the spectra analysis strongly focuses on the pre-edge features, which is the 1s to 3d dipole forbidden, quadruple transition [33, 34]. Besides, the Ti K-edge is more often used to study the bonding information by looking at absorption features well-above the edge (i.e. the extended X-ray absorption fine structure) [27, 34]. Herein, we limit our discussion on the Ti $L_{3,2}$-edge.

Figure 2 shows typical XANES spectra of TiO_2 at the Ti $L_{3,2}$-edge of anatase and rutile. In a Ti $L_{3,2}$-edge XANES, there are two sets of peaks, which belong to the L_3- and L_2-edge features. In each set, there is a sharp peak at lower energy (a and a') and a broad peak at higher energy (b and b'). Due to crystal field splitting, the conduction band of TiO_2 can actually be interpreted

http://dx.doi.org/10.5772/intechopen.72856

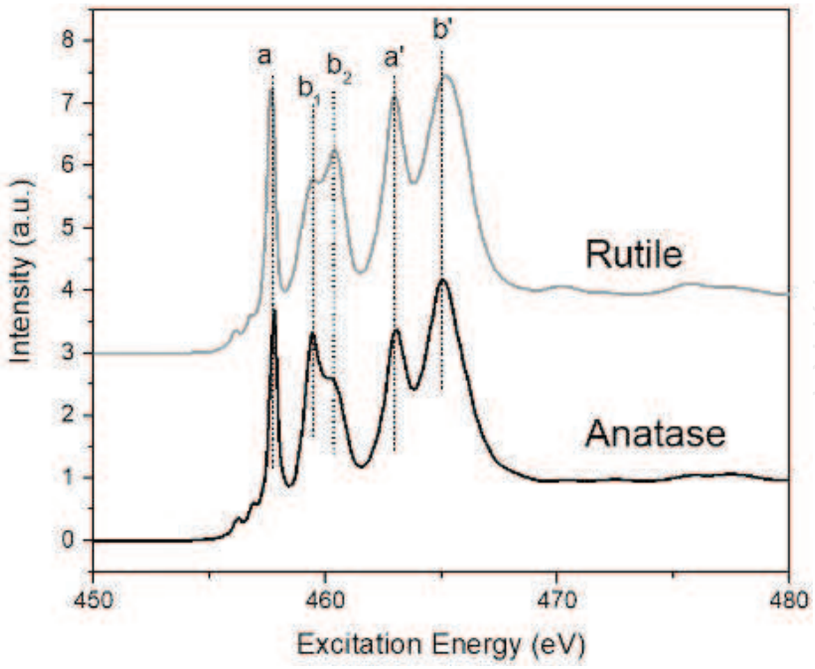

Figure 2. Typical XANES spectra of anatase and rutile TiO_2 at the Ti $L_{3,2}$-edge.

using a molecular orbital perspective. That is, in the octahedral field, the 3d orbitals are divided into two energy levels, t_{2g} and e_g, and they correspond to the a (a′) and b (b′) peaks, respectively. The e_g peak exhibits further splitting due to the reduced symmetry of O_h in anatase and rutile. For anatase, it is reduced to a D_{2d} symmetry, and for rutile, a D_{2h} symmetry, and in XANES, the difference is identified by the intensity ratio of the e_g doublet: anatase has a stronger peak b_1 and rutile has a stronger peak b_2.

The difference in crystal structure is also seen at the Ti L_2-edge. Due to the lifetime broadening and the background from the L_3 edge, the Ti L_2-edge does not exhibit features that are as sharp as the ones at the L_3-edge. However, we can still see that the b′ peak maximum shifts, so that the distance between a′ and b′ is larger in rutile than in anatase.

Based on these features, one could perform a composition analysis on any TiO_2 material, which contains a mixed phase of anatase and rutile using linear combination fit. We illustrate this with examples in the next section.

2.3. X-ray excited optical luminescence (XEOL)

XEOL is an X-ray photon-in, optical photon-out technique. It monitors the luminescence from a material under X-ray excitation. It differs from laboratory photoluminescence by its excitation source. When X-ray is used, electrons at deeper level are excited, leaving core hole, instead of just valence hole behind as in PL. The core hole is then filled with electrons at shallower levels, producing Auger electrons and a hole at an outer shell. The energetic electrons continue to travel in the solid, losing its energy and producing shallower core holes. This cascade process, often called “thermalization”, is repeated until the hole is created at the top of valence

band and fully thermalized electrons settling in the bottom of the conduction band. Then, the valence holes recombine with electrons at the bottom of the conduction band, producing luminescence via radiative excitonic de-excitation (near bandgap emission) and energy transfer to the impurity and defect states in the band gap (defect emission). **Figure 3** illustrates the process.

Since the energy of core electrons is element specific, XANES allows to track the absorption behavior of an element to provide element-specific local environment, a combined XEOL-XANES technique will allow us to build the relationship between the observed luminescence and the type of element that is responsible for it, and predict the chemical environment that leads to such luminescence. This is particularly valuable when analysing the role of dopant or structural defect luminescence [35, 36], as well as identifying the light-emitting component in a mixture of materials [24, 32].

Figure 4 shows a schematic layout of a synchrotron radiation endstation for conducting such experiment. We scan the incoming X-ray energy from below to above the absorption edge, the electron current generated by photoelectrons and secondary electrons is recorded as TEY, the emitted X-ray fluorescence photon is recorded as FY, and the amount of optical photon generated due to valence hole-conduction electron radiative recombination is recorded as photoluminescence yield (PLY). PLY can be collected for the entire wavelength region (200–900 nm) or at selected wavelengths. Using an energy/wavelength dispersive spectrometer, we could further gain a luminescence spectrum at each energy step. This will generate a 3D graph, which contains both the absorption behavior together with the associated luminescence. As shown in **Figure 5**, the color-coded map has a wavelength and excitation energy axis, the

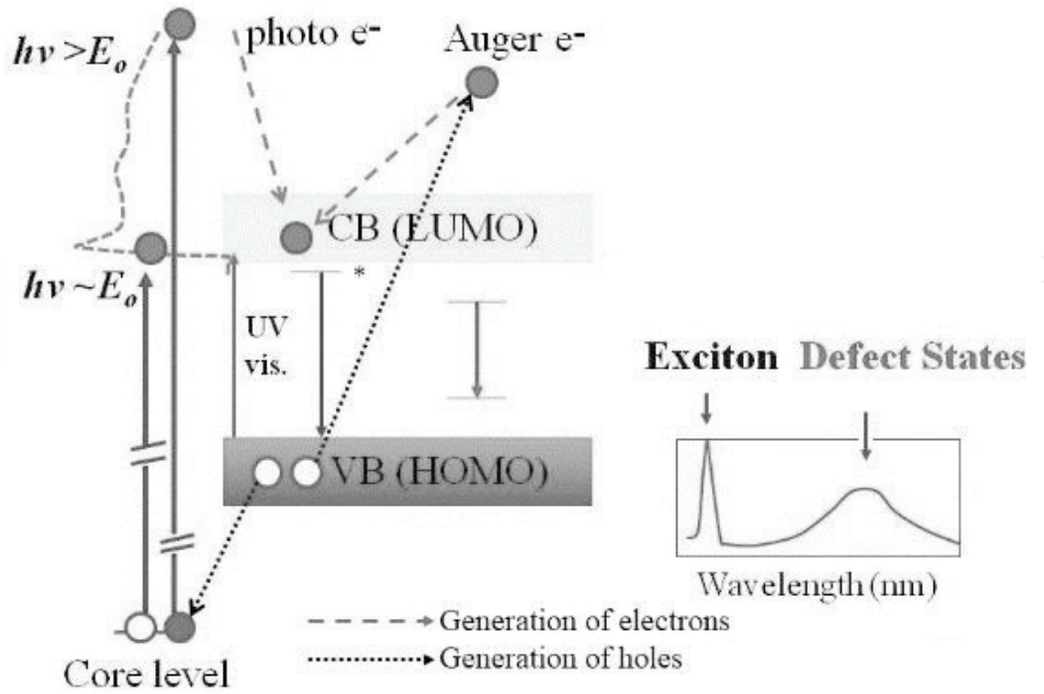

Figure 3. Illustration of a XEOL process from shallow core levels.

http://dx.doi.org/10.5772/intechopen.72856

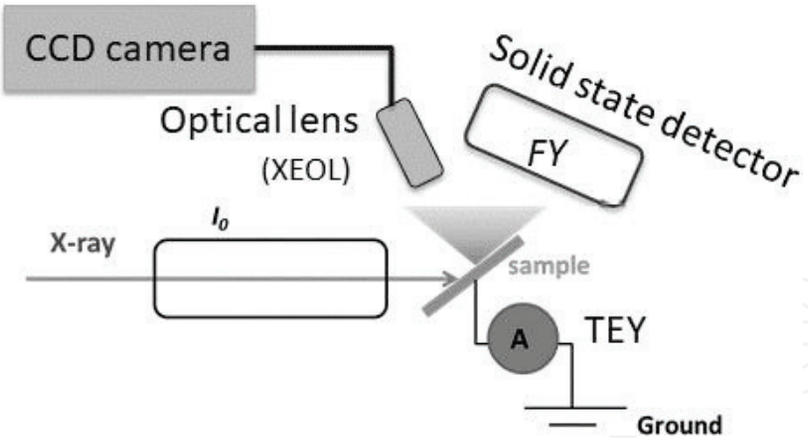

Figure 4. Experimental setup for XANES-XEOL measurements at synchrotron beamline endstation.

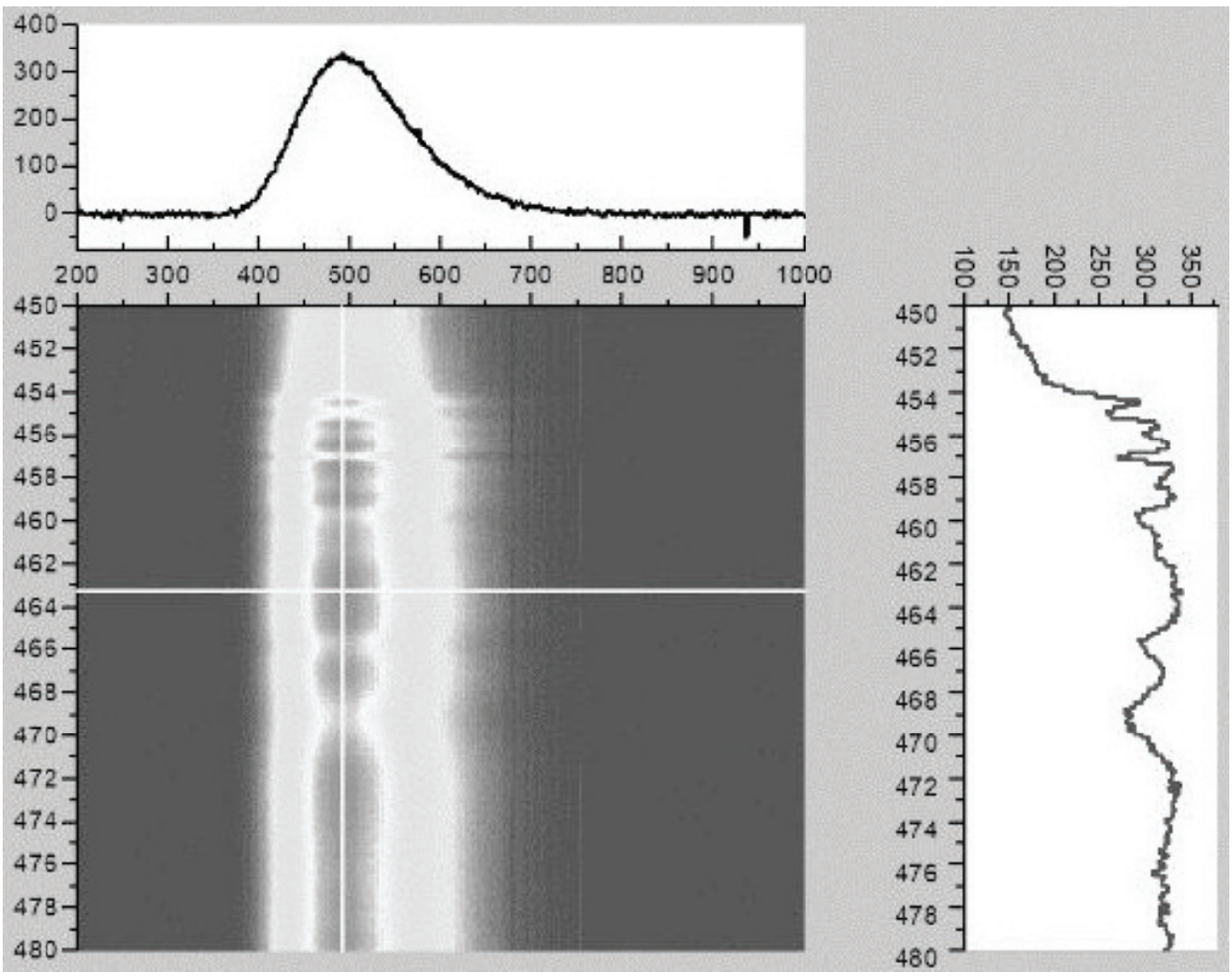

Figure 5. 2D XANES-XEOL map of TiO_2 nanowires. The x-axis is the luminescence wavelength, and the y-axis is the excitation photon energy. Color-coded z-axis is the luminescence intensity. A horizontal cut from the map (top panel) is XEOL at selected excitation energy and a vertical cut (right panel) is optical XANES of a selected luminescence wavelength.

vertical cut is a typical XANES spectrum, and the horizontal cut is a XEOL spectrum. In this way, both the change of absorption coefficient as well as the luminescence as a function of excitation energy can be tracked. This is the 2D XANES-XEOL.

3. Phase transformation and luminescence from TiO_2 nanotubes

TiO_2 NT made by anodization has an amorphous structure. Upon annealing, they crystalize into anatase structure, and when temperature increases further, phase transformation occurs and anatase gradually turns into rutile. The morphology of the nanotube retains at the amorphous and anatase phase, but entirely collapses when rutile phase dominates. **Figure 6** shows the morphology evolution of TiO_2 NT undergoing phase transformation [37]. The tubular structure gradually collapses and fused into bulky columns. The phase transformation in nanostructured TiO_2 has been reasonably well studied. Although the exact temperature for phase transformation to occur depends on material morphology, the anatase to rutile transformation is the common outcome when the calcination temperature increases.

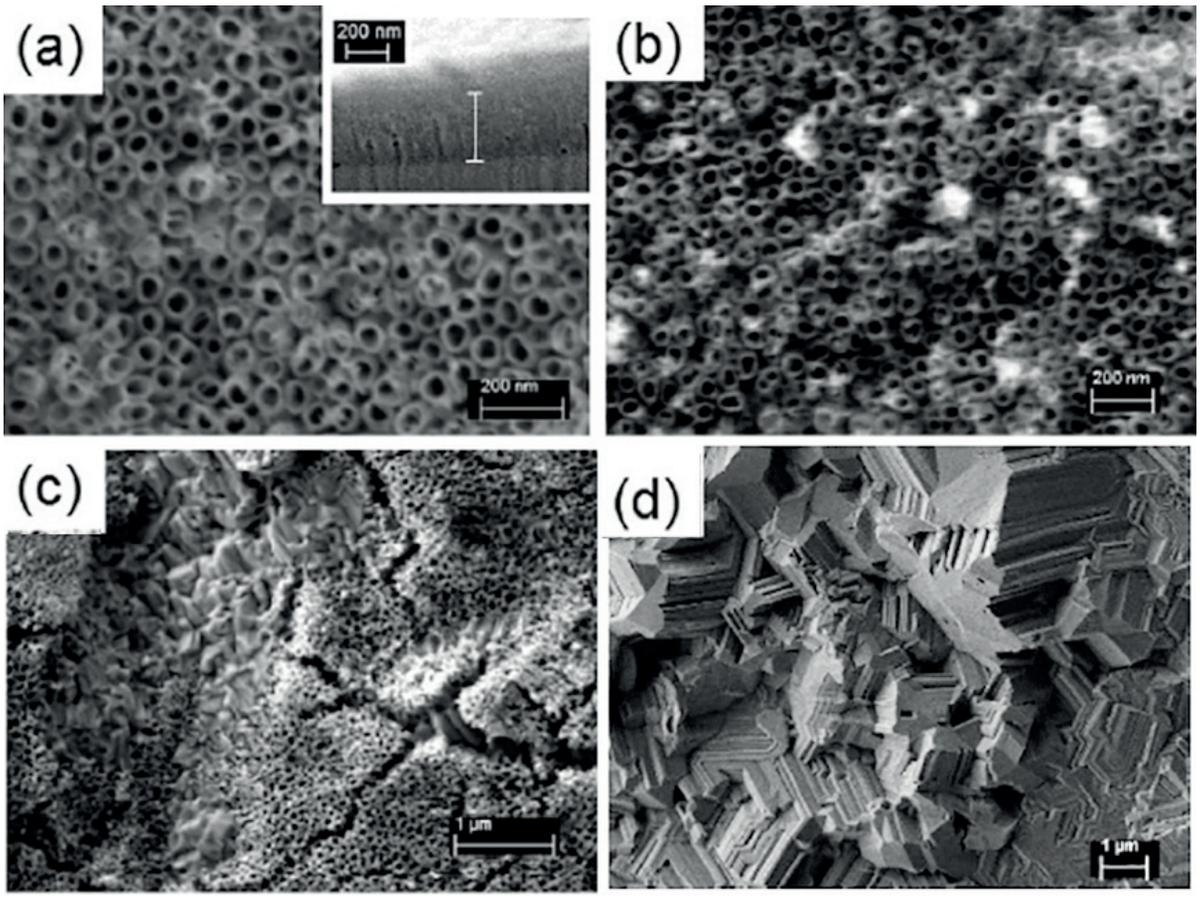

Figure 6. Scanning electron microscopy (SEM) images of TiO_2NT at different calcination temperatures. (a) as-prepared (inset is the cross section), (b) 500°C, (c) 650°C, and (d) 800°C. (Adapted from Ref. [37]).

http://dx.doi.org/10.5772/intechopen.72856

Figure 7a shows the evolution of XANES of TiO_2 NT as calcinated temperature increases. The as-prepared TiO_2 NT exhibits broad features due to its amorphous form. The e_g peak starts to show splitting at calcination temperature above 400°C indicating the formation of anatase phase, and the more intense b_1 than b_2 in the e_g splitting corresponds to anatase features. As the temperature increases, the b doublet persists, but the b_1/b_2 intensity varies. At 650°C, b_1 and b_2 exhibit similar intensities, indicating a mixed phase of roughly equal concentration. Higher temperature calcination produces a pure rutile phase. A linear combination fit can be conducted using XANES of anatase and rutile standards (e.g. **Figure 2**), as shown in **Figure 7b**.

Upon X-ray excitation, TiO_2 NT emits light. The luminescence properties of TiO_2 NT depend on both the crystal phases of the sample as well as the excitation energy. For nanostructures, it also depends on the size since the complete thermalization path in nanostructures can be truncated if the nanostructure is smaller than the thermalization path which can be tracked by the universal kinetic energy-dependent escape depth of electrons. For site specificity, we record the optical spectra (i.e. XEOL) using a fixed excitation energy just about the edge of interest, so that the site of interest can be preferentially excited. For example, XEOL can be recorded by selecting excitation energy above the O K-edge at 580 eV. In this circumstance, both the Ti 2p electrons and the O 1 s electrons can be excited, and more core holes can be thermalized, opening up both site-specific optical channels.

Figure 8 shows the XEOL profile of TiO_2 NT calcinated at elevated temperatures. Visible luminescence at the green region starts to appear when amorphous TiO_2 NT begins to crystallize into anatase, and the intensity gradually increases as the crystallinity improves. A minor high energy shift is also seen as the calcination temperature increases. The emergence of rutile phase is accompanied by an intense near-IR emission [37]. Its intensity increases with increased rutile concentration but the wavelength persists. The observation is in agreement with the ones reported using conventional laboratory PL [21, 22]. Both emissions are below the

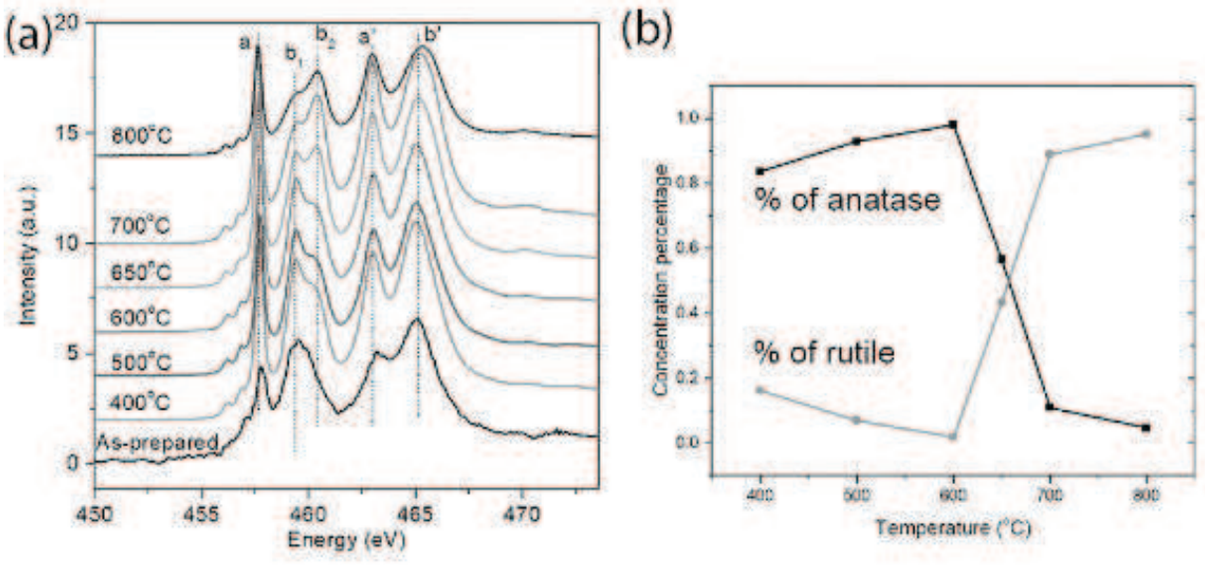

Figure 7. (a) XANES spectra of as-prepared and calcinated TiO_2 NT and (b) crystal phases' composition derived from linear combination fit.

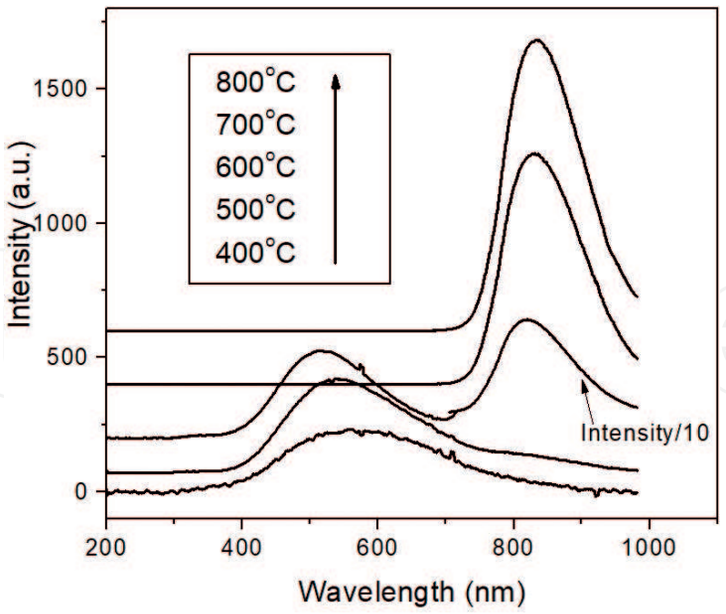

Figure 8. XEOL spectrum of TiO_2NT calcinated at different temperatures. (Adapted from Ref. [37]).

bandgap of anatase and rutile, so they are of defect origin. The visible emission is usually attributed to the oxygen vacancies as well as surface hydroxyl groups in the TiO_2 lattice, while the near-IR emission from rutile is from an intrinsic defect that the deep electron trap recombines with holes [22, 38]. Luminescence defected using X-ray as excitation source is similar to the one reported using laboratory PL; therefore, the experimental results obtained using the two techniques are comparable. However, XEOL can characterize luminescence from a second dimension, that is, for a fixed sample, tracking the evolution of luminescence intensity as a function of excitation energy.

Figure 9 shows the luminescence response of TiO_2 NT calcinated at 400, 600, and 700°C leading to the formation of anatase, mixed anatase and rutile, and rutile phase, respectively

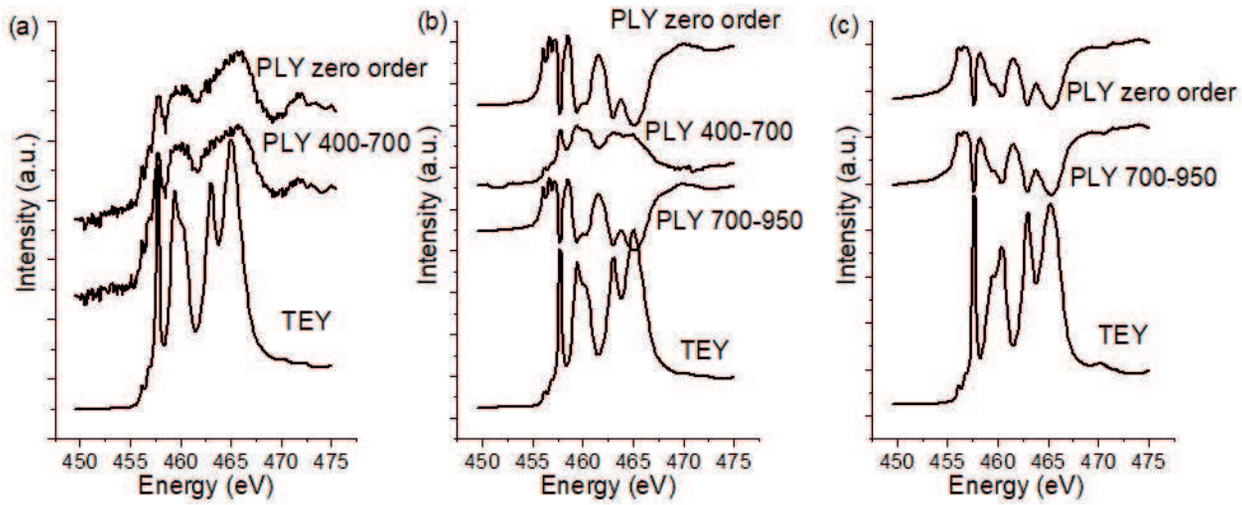

Figure 9. PLY spectra at the Ti $L_{3,2}$-edge in comparison with XANES obtained in TEY mode. (a) 400°C, (b) 600°C, and (c) 700°C. (Adapted from Ref. [37]).

with excitation energy across the Ti $L_{3,2}$- edge. This is done by the following: at each energy step, sum up the total optical photon counts (zero order PLY) or the photon counts within a selected wavelength window (partial PLY), and the final spectrum is a photon counts versus excitation energy plots. We can then compare the PLY spectra with the corresponding XANES spectra to obtain the relationship between structure and luminescence, so PLY is also called as the "optical XANES".

When TiO_2 NT only contains one emission peak at the green region, the PLY has the same profile as XANES, meaning that the radiative recombination site originates from the hybridized Ti 3d and O 2p states, and the intensity of the luminescence is proportional to the absorption coefficient of the element probed. This means, the decay of Ti 2p hole contributes to the luminescence positively. However, the PLY of the near IR emission from rutile retains all the features in XANES but completely inverted.

The inversion of PLY is not an unusual phenomenon. XEOL is produced by electron hole recombination near the bandgap via excitonic transition or energy transfer to defect states, but they are produced by thermalization following the decay of a core hole. The luminescence intensity can decrease if the energy transfer to the optical channel becomes less efficient, for example, the sampling depth decreases (increasing absorption) abruptly above the edge reducing the thermalization path. This is not uncommon for nanostructures since at these soft X-ray excitations, the specimen absorbs all the X-rays and above the absorption edge, the penetration depth of the X-ray reduces markedly, for example, just above and below the Ti L_3 edge, the one absorption length reduces by a factor of 6.5 meaning that above the edge most of the X-rays are absorbed in the near surface region (0.13 μm) as compared to the penetration depth just below (0.85 μm).[1] As a result, at excitation energy above the edge, a significant fraction of the energetic electrons created at or near the surface escape the sample without contributing fully to thermalization. If the luminescence has a bulk origin, like a deep level defect, hitting the absorption edge will decrease the luminescence.

Following this theory, the visible green band can be attributed to a surface-related defect of anatase origin, while the near IR emission is from bulk defect of rutile. This is also true when TiO_2 NT has more than one type of defect, as can be seen from the TiO_2 NT containing mixed phases, both visible green and near IR emission is present (**Figure 9b**). If we track each emission band individually using wavelength-selected PLY, we are able to distinguish between the optical responses from each emission band. As shown in **Figure 9b**, although the overall PLY exhibits a total inversion, the visible green component maintains the positive response. This means that the two emission bands have different origin and are from different region of the specimen. The surface-related defect is from the anatase phase, once it converts to rutile, only bulk defect is present. As a result, by using optical XANES (both total PLY and wavelength-selected PLY), one can investigate multicomponent emission separately and track the luminescence to its origin.

Since the degree of PLY inversion is thickness dependent, we can also correlate the observed emission to the location of the sample. In the abovementioned example, TiO_2 NT gradually

[1]Data obtained from X-ray calculator: http://henke.lbl.gov/optical_constants/

transform from anatase to rutile at elevated temperature, with the disappearing of the visible luminescence and emerging of the near IR emission. The PLY of visible emission (anatase phase) always exhibits a positive jump, meaning that anatase phase remains on the surface. On the other hand, as soon as rutile appears, it has an inverted PLY. If rutile appears on the surface of the tube, the thickness effect should be avoided, and PLY should have a normal positive jump. The observation suggests that the phase transformation of TiO_2 NT during calcination starts from the bottom to the top, from inside to the outside. This conclusion is later confirmed using scanning transmission X-ray microscopy that measures XANES from the top and the bottom of nanotubes separately in a mixed phase TiO_2 NT [39].

4. Luminescence from TiO_2 hierarchical nanostructures

When anodization is conducted at a high voltage (e.g. above 70 V), the nanotubular structure starts to break down due to the constant thinning of the tube walls, leading to the formation of a nanograss (NG)-nanotube (NT) hierarchical structure [20], shown in **Figure 10**. Although the formation of nanograss has long been observed, they are unzipped nanotube with reduced strain, and are often overlooked and treated as the by-product during TiO_2 NT formation. Recent findings suggest that the NG-on-NT hierarchical membrane exhibits interesting optical properties, which bring more potential applications of this material [40].

The most interesting observation from this structure is that the band emission is observed from the amorphous NG, while NT does not exhibit bandgap luminescence. TiO_2 is an indirect bandgap material, and the most commonly observed emission is from defects. A recent XEOL study on the amorphous TiO_2 NG, however, detected the weak but clear luminescence from it [20]. TiO_2 NG is excited with energy from below to above the Ti $L_{3,2}$-edge. As shown in **Figure 11**, the emission contains a broad peak centered at 3.30 eV when the excitation energy is below and well above the edge, while a second peak at 3.76 eV appears only when the

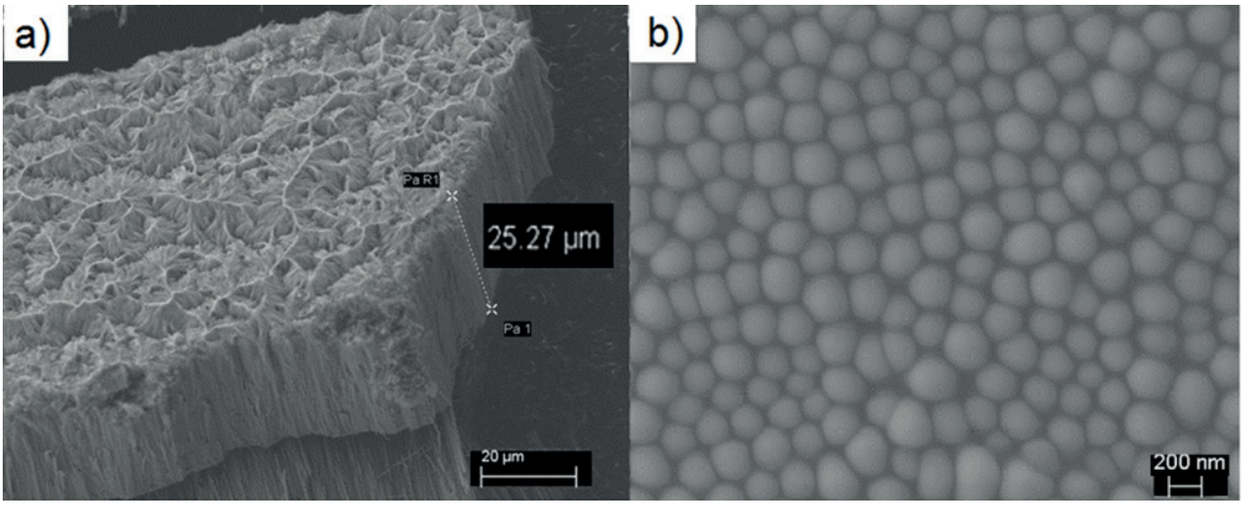

Figure 10. SEM images of nanograss-nanotube hierarchical structure. (a) Top/side view and (b) bottom view. (Adapted from Ref. [20]).

http://dx.doi.org/10.5772/intechopen.72856

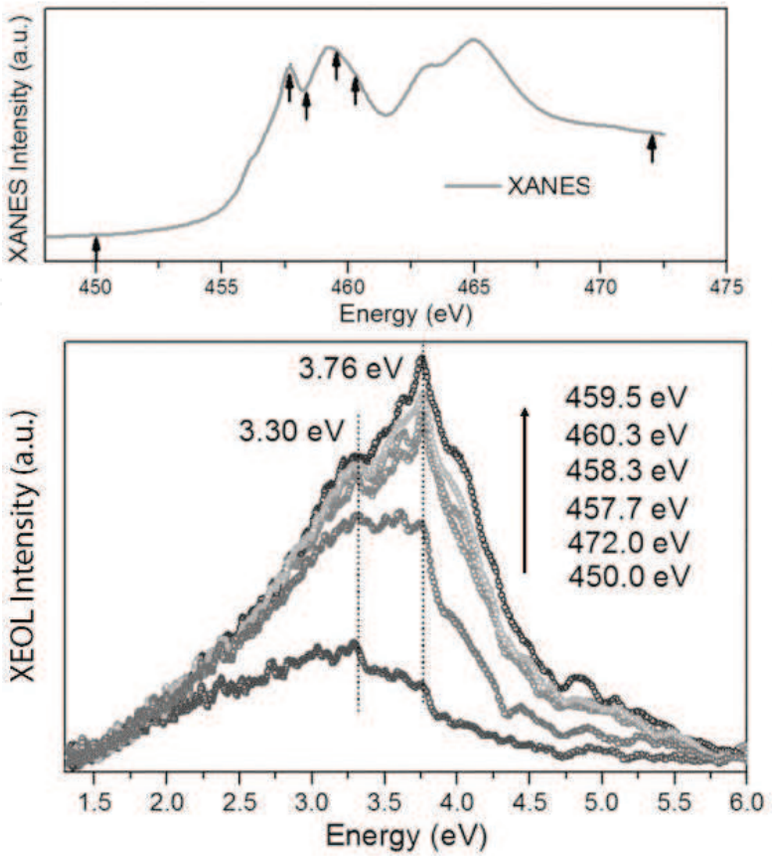

Figure 11. Top panel: Ti $L_{3,2}$-edge XANES of as-prepared nanograss. Bottom panel: XEOL spectra of nanograss under selected excitation energies indicated in the top panel. (Adapted from Ref. [20]).

energy just passes the edge. The 3.30 eV emission matches the value of bandgap measured by UV-vis absorption, and similar emission, although rare, has been reported from nanoparticles [41]. The 3.76 eV, however, is a unique band, and only appears when transition of the Ti 2p electron takes place. This band is hence a site-specific luminescence form NG and has been attributed to an up-conversion emission due to size effect [20].

Meanwhile, with two different nanostructures present, the hierarchical nanotubes exhibit unique phase transformation-induced light emission. A 2D XANES-XEOL study tracks the luminescence of NG and NT, after calcination at different temperatures, as a function of excitation energy is shown in **Figure 12** [40]. This map provides luminescence property in both energy space and wavelength space. Although anatase-to-rutile is a common trend at increased calcination temperature, NG can tolerate a much higher temperature (as high as 850°C) and remain anatase-like. The representative near-IR emission for rutile only shows up when the sample is calcinated at 900°C. In normal NT, a complete phase transformation usually occurs at temperature around 650°C [37].

Thus, 2D XANES-XEOL provides a clear view of the evolution of the luminescence, hence the structure. A hierarchical structure, which is made of the same material but of different morphologies, exhibits independent luminescence from the top and the bottom of the membrane.

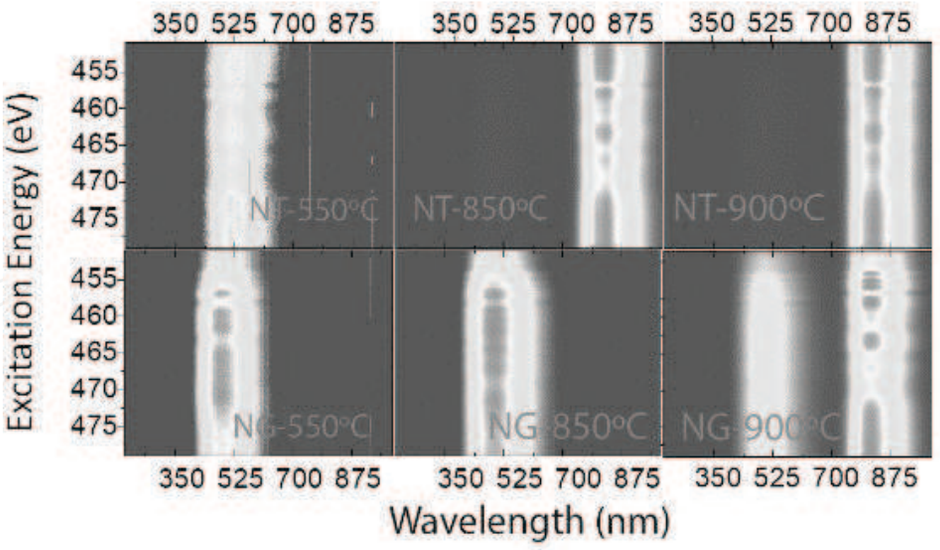

Figure 12. 2D XANES-XEOL plot of TiO_2 hierarchical structures annealed at different temperatures.

This technique sheds light on tracking the fabrication of light-emitting devices with spatially separated luminescence.

TiO_2 NT can also serve as a substrate for nanoparticle deposition. Noble metal loaded TiO_2 NT has been used in photocatalysis [42, 43] because the electron-hole recombination in TiO_2 can be effectively retarded with the presence of noble metal, leading to an enhanced photocatalytic efficiency [44]. The role of noble metal nanoparticles in modifying electronic structure of TiO_2 is investigated using XEOL-XANES. An example shows the study of Pd nanoparticles (PdNP)-loaded TiO_2 NT compared with pristine TiO_2 NT [19]. PdNP is deposited on TiO_2 NT by hydrothermal method, and the morphology is shown in **Figure 13a**.

Upon coating, the luminescence of TiO_2 NT changes. XEOL spectra, recorded with excitation energy above the O K-edge, are shown in **Figure 13b**. A decrease in intensity and a slight shift

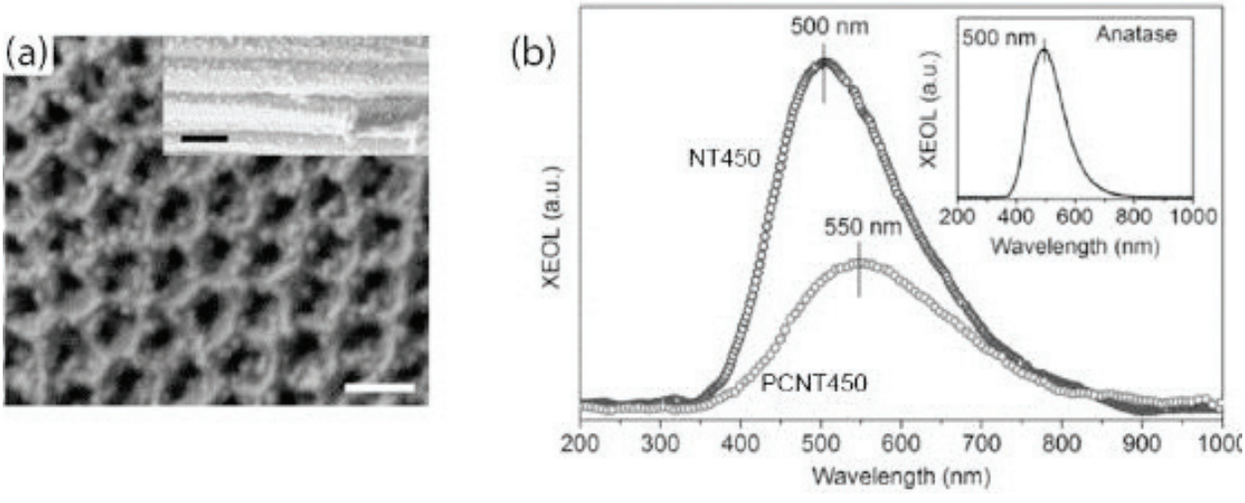

Figure 13. (a) The morphology of TiO_2NT after Pd deposition. (b) XEOL of TiO_2 NT with and without Pd nanoparticlet coating. (Adapted from Ref. [39]).

of the emission wavelength are observed in Pd-loaded TiO_2 NT. The presence of Pd has two roles such as modifies the defect states of TiO_2 on the surface and quenches the radiative recombination channel in TiO_2 by acting as an electron sink. Because of this, the photocatalysis efficiency can be improved with introducing PdNP.

5. Concluding remarks

TiO_2 NT is a versatile material. It could be directly used in batteries, photocatalysis, solar cells on their own, and it can also serve as substrate for further decorating of nanoparticles or bioactive compounds. Understanding the electronic structure of TiO_2 NT-based materials and controlling their electronic and optical properties is hence crucial for integrating them into practical application. Both anatase and rutile nanostructures have their characteristic luminescence at visible green and near IR regions, respectively. The visible green luminescence in NT is of a surface origin, and it is highly sensitive to surface defect and surface modification. Near IR emission, on the other hand, is of bulk origin of rutile. It is independent of material morphology and always appears as long as rutile phase is present, even in a mixed structure. Thus XEOL in combination with XANES is a unique and powerful technique which tracks the relationship of the observed luminescence and the specific local chemical structure that is responsible for it. It is hence useful in analyzing the luminescence origin of novel TiO_2 nanostructures and related materials.

Author details

Lijia Liu[1] and Tsun-Kong Sham[2]*

*Address all correspondence to: tsham@uwo.ca

1 Jiangsu Key Laboratory for Carbon-Based Functional Materials and Devices, Institute of Functional Nano and Soft Materials, Soochow University, Suzhou, Jiangsu, China

2 Department of Chemistry, University of Western Ontario, London, ON, Canada

References

[1] O'Regan B, Gratzel M. Synthesis of nanocrystalline titanium dioxide dye sensitized solar cell. Nature. 1991;**353**:737

[2] Fujishima A, Honda K. Electrochemical photolysis of water at a semiconductor electrode. Nature. 1972;**238**:37

[3] Varghese OK, Gong D, Paulose M, Ong KG, Dickey EC, Gremes CA. Extreme changes in the electrical resistance of titania nanotubes with hydrogen exposure. Advanced Materials. 2003;**15**:624

[4] Zhou JG, Fang HT, Maley JM, Murphy MW, Ko JYP, Cutler JN, Sammynaiken R, Sham TK, Liu M, Li F. Electronic structure of TiO_2 nanotube arrays from X-ray absorption near edge structure studies. Journal of Materials Chemistry. 2009;**19**:6804

[5] Tsuchiya H, Macak JM, Muller L, Kunze J, Muller F, Greil P, Virtanen S, Schmuki P. Hydroxyapatite growth on anodic TiO_2 nanotubes. Journal of Biomedical Materials Research. Part A. 2006;**77**:534

[6] Buin A, Constas S, Sham TK. Mechanisms of phase transformations of TiO_2 nanotubes and nanorods. Journal Physical Chemistry C. 2011;**115**:22257

[7] Li J, Wan W, Zhou H, Li J, Xu D. Hydrothermal synthesis of TiO_2(B) nanowires with ultrahigh surface area and their fast charging and discharging properties in Li-ion batteries. Chemical Communications. 2011;**47**:3439

[8] Aravindan V, Shubha N, Ling C, Madhavi S. Constructing high energy density non-aqueous Li-ion capacitors using monoclinic TiO_2-B nanorods as insertion host. Journal of Materials Chemistry A. 2013;**1**:6145

[9] Zhang J, Li M, Feng Z, Chen J, Li C. UV Raman spectroscopic study on TiO_2. I. Phase transformation at the surface and in the bulk. The Journal of Physical Chemistry. B. 2006;**110**:927

[10] Shannon RD, Pask JA. Kinetics of the anatase-rutile. Journal of the American Ceramic Society. 1965;**48**:391

[11] Gribb AA, Banfield JF. Particle size effects on transformation kinetics and phase stability in nanocrystalline TiO_2. American Mineralogist. 1997;**82**:717-728

[12] Gouma PI, Mills MJ. Anatase-to-rutile transformation in titania powders. Journal of the American Ceramic Society. 2001;**84**:619-622

[13] Ghosh TB, Dhabal S, Datta AK. On crystallite size dependence of phase stability of nanocrystalline TiO_2. Journal of Applied Physics. 2003;**94**:4577-4582

[14] Yan M, Chen F, Zhang J, Anpo M. Preparation of controllable crystalline titania and study on the photocatalytic properties. Journal of Physical Chemistry B. 2005;**109**:8673-8678

[15] Li G, Gary KA. The solid-solid interface: Explaining the high and unique photocatalytic reactivity of TiO_2-based nanocomposite materials. Chemical Physics. 2007;**339**:173-179

[16] Roy P, Berger S, Schmuki P. TiO_2 nanotubes: Synthesis and applications. Angewandte Chemie, International Edition. 2011;**50**:2904-2939

[17] Lee K, Zazare A, Schnuki P. One-dimensional titanium dioxide nanomaterials: Nanotubes. Chemical Reviews. 2014;**114**:9385-9454

[18] Ali G, Kim HJ, Kim JJ, Cho SO. Controlled fabrication of porous double-walled TiO_2 nanotubes via ultraviolet-assisted anodization. Nanoscale. 2014;**6**:3612

[19] Li J, Sham TK, Ye Y, Zhu J, Guo J. Tracking the local effect of fluorine self-doping in anodic TiO_2 nanotubes. Journal of Physical Chemistry C. 2015;**119**:2222-2230

[20] Liu L, Li J, Sham TK. Near-band-gap luminescence from TiO_2 nanograss-nanotube hierarchical membranes. Canadian Journal of Chemistry. 2015;**93**:106-112

[21] Knorr FJ, Zhnag D, McHale JL. Influence of $TiCl_4$ treatment on surface defect photoluminescence in pure and mixed-phase nanocrystalline TiO_2. Langmuir. 2007;**23**:8686-8690

[22] Shi J, Chen J, Feng Z, Chen T, Lian Y, Wang X, Li C. Photoluminescence characteristics of TiO_2 and their relationship to the photoassisted reaction of water/methanol mixture. Journal of Physical Chemistry C. 2007;**111**:693-699

[23] Wang Z, Gou XX, Sham TK. 2D XANES-XEOL mapping: Observation of enhanced band gap emission from ZnO nanowire arrays. Nanoscale. 2014;**6**:6531-6536

[24] Ward MJ, Han WQ, Sham TK. 2D XAFS-XEOL mapping of $Ga_{1-x}Zn_xN_{1-x}O_x$ nanostructured solid solutions. Journal of Physical Chemistry C. 2011;**115**:20507-20514

[25] Thomas JM, Sankar G. The role of synchrotron-based studies in the elucidation and design of active sites in titanium–silica epoxidation catalysts. Accounts of Chemical Research. 2001;**34**:571-581

[26] Germack DS, Chan CK, Hamadani BH, Ritcher LJ, Fischer DA, Gundlach DJ, DeLongchamp DM. Substrate-dependent interface composition and charge transport in films for organic photovoltaics. Applied Physics Letters. 2009;**94**:233303

[27] Wang D, Liu L, Sun X, Sham TK. Observation of lithiation-induced structural variations in TiO_2 nanotube arrays by X-ray absorption fine structure. Journal of Materials Chemistry A. 2015;**3**:412-419

[28] Gorlin Y, Lassalle-Kaiser B, Benck JD. In situ X-ray absorption spectroscopy investigation of a bifunctional manganese oxide catalyst with high activity for electrochemical water oxidation and oxygen reduction. Journal of the American Chemical Society. 2013;**135**: 8525-8534

[29] Yoon WS, Grey CP, Balasubramanian M, Yang XQ, McBreen J. In situ X-ray absorption spectroscopic study on $LiNi0.5Mn0.5O_2$ cathode material during electrochemical cycling. Chemistry of Materials. 2003;**15**:3161-3169

[30] Kinyangi J, Solomon D, Liang BI, Lerotic M, Wirick S, Lehmann J. Nanoscale biogeocomplexity of the organomineral assemblage in soil. Soil Science Society of America Journal. 2006;**70**:1708-1718

[31] Lawrence JR, Swerhone GDW, Leppard GG, Araki T, Zhang X, West MM, Hitchcock AP. Scanning transmission X-ray, laser scanning, and transmission electron microscopy mapping of the exopolymeric matrix of microbial biofilms. Applied and Environmental Microbiology. 2003;**69**:5543-5554

[32] Wang ZQ, Wang W, Sham TK, Yang SG. Origin of luminescence from ZnO/CdS core/shell nanowire arrays. Nanoscale. 2014;**6**:9783-9790

[33] Kim KT, Ali G, Chung KY, Chong SY, Yashiro H, Sun YK, Lu J, Amine K, Myung ST. Anatase titania nanorods as an intercalation anode material for rechargeable sodium batteries. Nano Letters. 2014;**14**:416-422

[34] Okumura T, Fukutsuka T, Yanagihara A, Orikasa Y, Arai H, Ogumi Z, Uchimoto Y. Electronic and local structural changes with lithium-ion insertion in TiO_2-B: X-ray absorption spectroscopy study. Journal of Materials Chemistry. 2011;**21**:15369-15377

[35] Ko JYP, Yiu YM, Liang HB, Sham TK. X-ray absorption and luminescence studies of Ba2Ca(BO_3)2:Ce_3+/Na+ phosphors. The Journal of Chemical Physics. 2010;**132**:234701

[36] Wang DN, Yang JL, Li XF, Wang JJ, Li RY, Cai M, Sham TK, Sun XL. Observation of surface/defect states of SnO_2 nanowires on different substrates from X-ray excited optical luminescence. Crystal Growth & Design. 2012;**12**:397-402

[37] Liu L, Chan J, Sham TKJ. Calcination-induced phase transformation and accompanying optical luminescence of TiO_2 nanotubes: An X-ray absorption near-edge structures and X-ray excited optical luminescence study. Physical Chemistry C. 2010;**114**:21353-21359

[38] Wang X, Feng Z, Shi J, Jia G, Shen S, Zhou J, Li C. Trap states and carrier dynamics of TiO(2) studied by photoluminescence spectroscopy under weak excitation condition. Physical Chemistry. 2010;**12**:7083-7090

[39] Li J, Wang Z, Wang J, Sham TK. Unfolding the anatase-to-rutile phase transition in TiO_2 nanotube using X-ray spectroscopy and spectromicroscopy. Journal of Physical Chemistry C. 2016;**120**:22079-22087

[40] Li J, Liu L, Sham TK. 2D XANES-XEOL spectroscopy studies of morphology-dependent phase transformation and corresponding luminescence from hierarchical TiO_2 nanostructures. Chemistry of Materials. 2015;**27**:3021-3029

[41] Abazovic ND, Comor MI, Dramicanin MD, Jovanovic DJ, Ahrenkiele SP, Nedeljkovic JM. New paradigms for active site engineering in titanium dioxide photocatalysts. Journal of Physical Chemistry B. 2006;**110**:25366

[42] Li XH, Chen GY, Yang LB, Lin Z, Liu JH. Multifunctional Au-coated TiO_2 nanotube arrays as recyclable SERS substrates for multifold organic pollutants detection. Advanced Functional Materials. 2010;**20**:2815-2824

[43] Lin CH, Lee CH, Chao JH, Kuo CY, Cheng YC, Huang WN, Chang HW, Huang YM, Shih MK. Photocatalytic generation of H_2 gas from neat ethanol over Pt/TiO_2 nanotube catalysts. Catalysis Letters. 204;**98**:61–66

[44] Ye MD, Gong JJ, Lai YK, Lin CJ, Lin ZQ. High-efficiency photoelectrocatalytic hydrogen generation enabled by palladium quantum dots-sensitized TiO_2 nanotube arrays. Journal of the American Chemical Society. 2012;**134**:15720-15723